Materials Chemistry and Physics 209 (2018) 76–85

Contents lists available at ScienceDirect

Materials Chemistry and Physics

journal homepage: www.elsevier.com/locate/matchemphys

Electrodeposition study of polypyrrole-heparin and polypyrrole-salicylate coatings on Nitinol

D.O. Flamini [a, *], M.I. Valle [b], M.J. Sandoval [b], V.L. Massheimer [b], S.B. Saidman [a]

[a] Instituto de Ingeniería Electroquímica y Corrosión (INIEC), Departamento de Ingeniería Química, Universidad Nacional del Sur, Av. Alem 1253, 8000, Bahía Blanca, Argentina

[b] Cátedra de Bioquímica Clínica II, Departamento de Biología, Bioquímica y Farmacia, Instituto de Ciencias Biológicas y Biomédicas del Sur (INBIOSUR), Consejo Nacional de Investigaciones Científicas y Técnicas (CONICET), Universidad Nacional del Sur (UNS), San Juan 670, B8000ICN, Bahía Blanca, Argentina

HIGHLIGHTS

- PPy films containing Hep, Sa or both anions were formed onto NiTi alloy.
- The morphology of the formed film depends of the dopant species.
- The presence of Hep and Sa in the PPy film improve the anticoagulant properties.
- The PPy film containing Hep and Sa has the best pitting corrosion protection.

ARTICLE INFO

Article history:
Received 11 July 2017
Received in revised form
26 December 2017
Accepted 21 January 2018

Keywords:
Nitinol
Heparin
Salicylate
Polypyrrole
Anticoagulant activity

ABSTRACT

Polypyrrole (PPy) films containing heparin (Hep), salicylate (Sa) or both anions were electrochemically deposited as single layers or bilayers onto Nitinol (NiTi) alloy. The PPy deposition onto the bare alloy was achieved through an anodic electropolymerization in the presence of the anions. The aim of this study was to determine the influence of the electrosynthesis parameters (electrolyte nature and monomer and electrolyte concentrations) on the electroforming mechanism and morphology of the PPy. The PPy coating containing Hep and Sa not only presents a very good anticoagulant activity but also presents excellent anticorrosive properties in Ringer's solution.

© 2018 Elsevier B.V. All rights reserved.

1. Introduction

The equiatomic alloy containing Ni and Ti elements, better known as Nitinol (NiTi), is widely used as a biomaterial in a great number of biomedical applications such as orthodontic wires, cardiovascular and nephrology stents, bone implants and as a surgical material [1–3]. Its high corrosion resistance and biocompatibility with the human body can be attributable to an oxide layer mainly composed of TiO_2 with a small amount of NiO on the alloy surface [4]. The main problem related to the use of Nitinol as implant material is the release of allergenic and toxic Ni^{2+} ions into the human body fluids [4–6]. The solution to this problem has stimulated researchers to develop different treatments to modify its surface.

Polypyrrole (PPy) is an attractive organic coating for a large number of biological and biomedical applications due to its biocompatibility with the human body tissues [7]. The electrochemical synthesis of hollow rectangular microtubes of PPy in salicylate (Sa) solutions on different metallic biomaterials, has been carried out successfully in our laboratory [8,9]. Sodium salicylate (NaSa) is a non-steroidal anti-inflammatory drug (NSAID) used in medicine as analgesic and anti-inflammatory agent. Moreover, Sa exhibits antiplatelet activity by reducing activation, adhesion and aggregation of platelets [10].

On the other hand, is widely known that heparin (Hep) has anticoagulant properties [11]. Hep is a linear polysaccharide

* Corresponding author. Instituto de Ingeniería Electroquímica y Corrosión (INIEC), Departamento de Ingeniería Química, Universidad Nacional del Sur, Av. Alem 1253, 8000 Bahía Blanca, República Argentina.
E-mail address: dflamini@uns.edu.ar (D.O. Flamini).

https://doi.org/10.1016/j.matchemphys.2018.01.065
0254-0584/© 2018 Elsevier B.V. All rights reserved.

composed of repeated units of uronic acid, containing an *o*-sulfate group at the C-2 position, and D-glucosamine, usually *N*-sulfated with an additional *o*-sulfate group at the C-6 position [12]. The general structure, although no always identical, is represented as shown below:

It produces its major anticoagulant effect by inactivating thrombin and activated factor X (factor X_a) through an antithrombin (AT)-dependent mechanism. Heparin binds to AT through a high-affinity pentasaccharide, which is present on about a third of heparin molecules. For inhibition of thrombin, heparin must bind to both the coagulation enzyme and AT, whereas binding to the enzyme is not required for inhibition of factor X_a [13]. The combination of NSAID with anticoagulant drugs as Hep enhances their anticoagulant properties.

Electropolymerization is an interesting method to develop a PPy coating, wherein the pyrrole (Py) monomer is dissolved in aqueous or organic solvent containing an anionic dopant [14]. The monomer is oxidized onto the metallic surface by a simple anodic oxidation to produce the polymer films. In this simple step the anionic dopant is incorporated into the polymeric matrix in order to assure the electrical neutrality of the coating. Moreover, PPy has the ability to incorporate bioactive molecules, such as Hep, to improve its compatibility with the human body [15]. The electrochemical synthesis of PPy in aqueous solutions containing Hep as a bulky anionic dopant has been studied by different authors over different metallic substrates in order to assess the anticoagulant ability of the composite coating [16–22].

The formation of PPy coatings onto NiTi alloy doped with different concentrations of Hep was studied in this work. Furthermore, the formation of a composite coating constituted by a first layer of hollow rectangular microtubes of PPy doped with Sa and a second layer of PPy that contains Hep was investigated. The electrosynthesis of a PPy layer in a solution containing both dopants (Hep and Sa) was also carried out. Finally, the anti-corrosive properties of the different PPy coatings in Ringer solution as well as their anticoagulant ability in blood plasma were determined.

2. Material and methods

A cylindrical rod of NiTi alloy of 3.5 mm in diameter axially mounted in a Teflon holder was used as working electrode (WE) in the electrochemical experiments. The exposed area of the WE was 0.0962 cm^2 and its chemical composition (in wt. %) is: 55.8 Ni, 0.05 O, 0.02 C and Ti balance. In addition, NiTi square sheets of 1 cm^2 of exposed area were used as WE on the coagulation experiments. Before each experiment, the WE was abraded with SiC papers down to 1200 grit finish, then degreased with acetone and finally washed with triply distilled water. Then, the WE was immediately transferred to an electrochemical cell. A large Pt sheet was used as counter electrode and a saturated calomel electrode (SCE) was used as reference electrode. All potential values in this work are referred to SCE. Electrochemical experiments were performed in a Metrohm cell of 20 cm^3 employing a potentiostat-galvanostat PAR Model 273A. Electrochemical impedance spectroscopy (EIS) measurements were made using a potentiostat-galvanostat VoltaLab 40 Model PGZ301. The frequency was changed from 10 kHz to 100 mHz and a signal amplitude of 10 mV was used.

PPy films were obtained under potentiostatic conditions at 0.9, 1.0 and 1.5 V (SCE) during different polarization times (600 and 1800 s) from different solutions containing the monomer (pyrrole (Py, Sigma Aldrich)), previously distilled under vacuum before use.

The following solutions were used for the electrochemical synthesis:

1) x g L^{-1}Hep + 0.5 M Py, with x = 0.2, 0.3 y 0.4.
2) 0.5 M NaSa + 0.5 M Py
3) x g L^{-1}Hep + 0.5 M NaSa + 0.5 M Py, with x = 0.2 y 0.4.

Sodium salicylate and heparin sodium salt from porcine intestinal mucosa (Grade I-A with an activity of 180 USP units mg^{-1} and molecular weight between 17000 and 19000 Da) were purchased from Sigma-Aldrich and used as received.

The corrosion behavior of the coatings was evaluated by monitoring the open circuit potential (OCP) with time, linear sweep voltammetry (LSV), potentiostatic and EIS measurements in Ringer's solution (0.147 M NaCl, 0.00432 M $CaCl_2$ and 0.00404 M KCl), which is frequently used to simulate biological environment.

Tafel plots were used to determine the electrochemical parameters (anodic Tafel slope (βa), cathodic Tafel slope (β_c), corrosion potential (E_{corr}) and corrosion current density (i_{corr})). The i_{corr} was obtained by extrapolation of the linear part of the anodic and/or cathodic branches to E_{corr}.

Ni and Ti released concentrations in Ringer solution were analyzed using an inductively coupled plasma atomic emission spectrometer (ICP-AES) (ICPE 9000 - Shimadzu Corporation, Japan).

A scanning electron microscope (SEM) model LEO-EVO 40-XVP equipped with an X-ray energy dispersive system (EDX) model X-Max 50 (Oxford) was used for morphology characterization of the coatings. A fine carbon layer was used to improve the imaging of the samples.

The Fourier Transform Infrared (FT-IR) spectra of the different electrodeposited PPy films were recorded as KBr pellets in the 4000 to 400 cm^{-1} range on a Thermo Scientific Nicolet iS50 FTIR-NIR spectrometer.

The effect of PPy films doped with Hep, Sa or the combination of both anions on blood coagulation and platelet aggregation (PA) was evaluated. To that end, platelet poor plasma (PPP) was used in thrombin time (TT) and fibrinogen (F) measurements, and platelet rich plasma (PRP) for PA assays. PRP was obtained by centrifugation of citrated (0.38%) whole human blood at 240 × g for 20 min at room temperature, and PPP was obtained after centrifugation at 1200 × g for 15 min. Platelet concentration was adjusted to 3×10^{-8} cells mL^{-1}. Citrate was employed in order to remove calcium ions that are essential for blood coagulation. Slices were placed in a multiwell plate and incubated with PPP or PRP during 35 min at 37 °C with gentle movement. Immediately after, aliquots were taken for haemostatic assays performed as described below.

Coagulation tests (TT and F) were performed at 37 °C using Stago ST2 Coagulometer and commercial available kits (Wiener Lab, Argentina). TT test quantified the time taken for coagulation of an aliquot of PPP after thrombin addition. The results were expressed in seconds and represent the means of three independent experiments performed by duplicate.

F assay measured the plasmatic F content. To that end, thrombin was added to aliquots of PPP, immediately after the time taken for clot was determined, and the F concentration was quantified using a standardized preparation of F. Coagulation rate is inversely proportional to the F plasma concentration. The results were expressed in mg dL^{-1}, and represent the means of three independent experiments performed by duplicate.

PA was measured using a turbidimetric technique. Aliquots (285 μL) of each PRP were taken and set in an aggregometer cuvette (Chronolog 430) and prewarmed at 37 °C. Platelet aggregation was initiated by addition of 15 μL of 2×10^{-5} M ADP. Changes in light transmission were recorded for 5 min. Maximal PA (100%) was considered that induced by PRP alone. Results were expressed as percent of inhibition of PA (IPA).

3. Results and discussion

3.1. Electrochemical synthesis of PPy films

The electrochemical polymerization on NiTi alloy was carried out in solutions containing the monomer (0.5 M Py) and different Hep concentrations (0.2, 0.3 and 0.4 g L^{-1}). A cyclic voltammetry (CV) was performed from - 1.20 to 1.70 V (SCE) at a scan rate of 0.05 V s^{-1} (Fig. 1). It can be observed in this figure that the anodic process related to Py oxidation begins around 1.0 V (SCE). The oxidation potential of Py shifted to more negative values when Hep concentration was increased. Repetitive cycling results in a progressive increase in the charge of the redox waves which appear at more negative potential than that corresponding to the monomer oxidation. These curves are associated with polymeric deposits because, after cycling, a black and uniform PPy layer covering the entire substrate was observed. Two reduction peaks at 0.1 V (SCE) and the other at - 1.0 V (SCE) were observed (Fig. 1 (d)) in the negative potential scan of the first cycle, which could be attributed to the expulsion of a fraction Hep polyanion and insertion of Na^+ ions into the polymer, in order to maintain charge neutrality. Considering the large volume of the heparin molecule, it can be said that part of these molecules are retained in the polymer matrix, as was previously demonstrated by Zhou et al. [16].

If the CV is carried out in a 0.5 M Py solution containing 0.5 M NaSa and 0.2 g L^{-1} Hep (Fig. 2), a considerable increase in the redox charge of the polymer occurs, due to high concentration of Sa anion.

More homogeneous PPy films with a higher coating degree were also synthesized onto NiTi alloy under potentiostatic conditions. A constant potential of 1.0 or 1.5 V(SCE) was applied in solutions of 0.50 M Py that contained different Hep concentration (0.2, 0.3 and 0.4 g L^{-1}) with and without the presence of NaSa (0.50 M). For simplification the films synthesized under potentiostatic control on NiTi alloy in solutions containing Hep and NaSa will be named as PPy_{xHep} and PPy_{ySa}, respectively; where x represents the

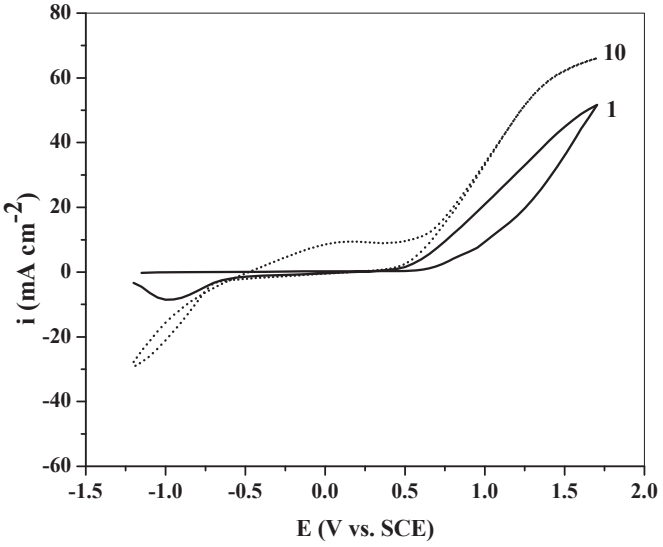

Fig. 2. CV obtained for NiTi alloy in the presence of 0.50 M Py solution containing 0.2 g L^{-1} Hep and 0.5 M NaSa. The first (full line) and tenth (dotted lined) cycles are displayed. Scan rate: 0.05 V s^{-1}.

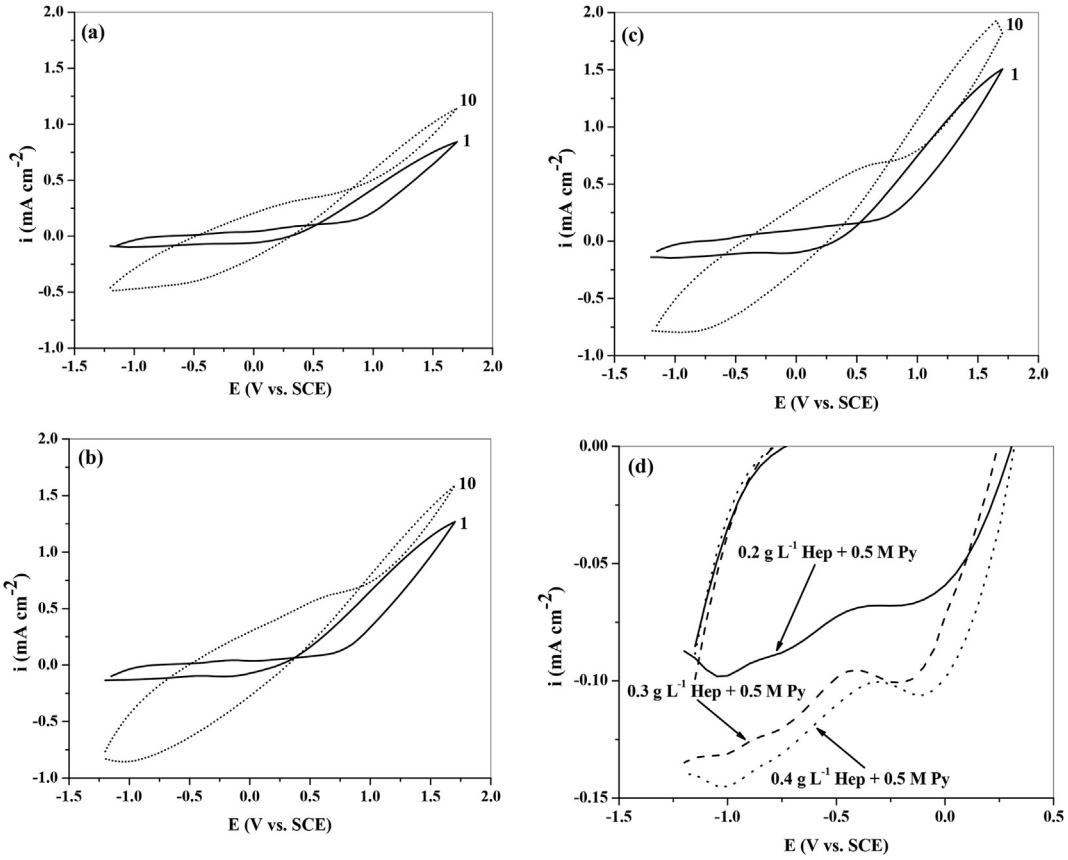

Fig. 1. CV obtained for NiTi alloy in the presence of 0.50 M Py solution containing different Hep concentration: (a) 0.2, (b) 0.3 and (c) 0.4 g L^{-1}. The first (full line) and tenth (dotted lined) cycles are displayed. Scan rate: 0.05 V s^{-1}. In the case of curve (d) the first cycle in the cathodic region of the CV was showed magnified.

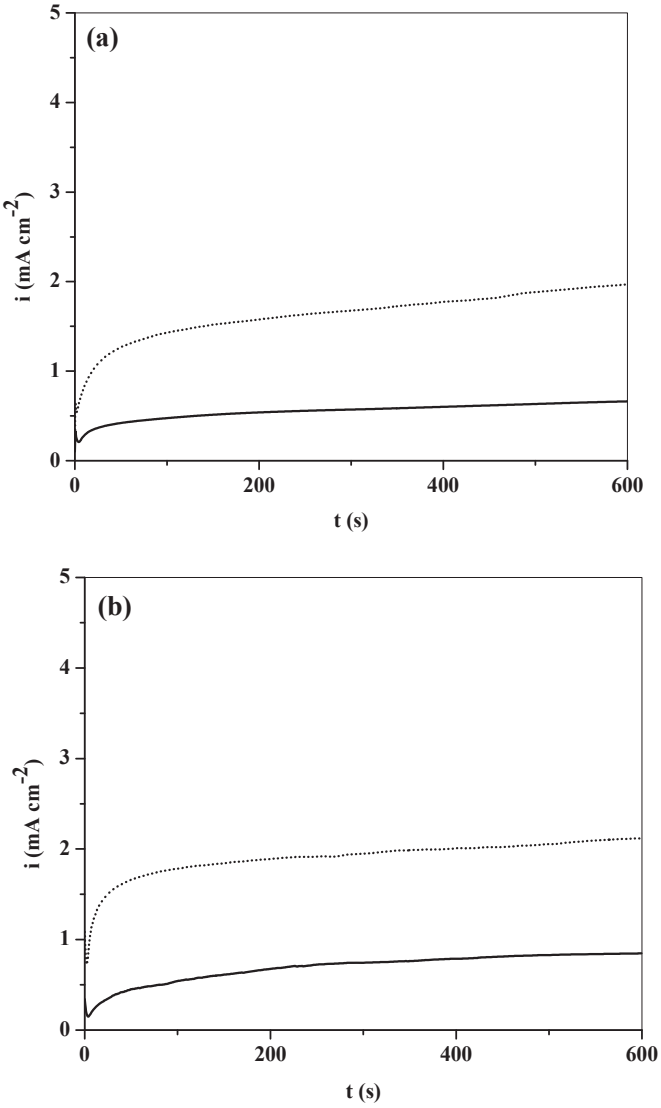

Fig. 3. i versus t transients obtained for NiTi alloy in the presence of 0.50 M Py solution containing different Hep concentration: (a) 0.2, (b) 0.3 and (c) 0.4 g L^{-1}. In solid line the transients obtained at 1.0 V (SCE) and in dotted line the transients obtained at 1.5 V (SCE) for all Hep concentrations.

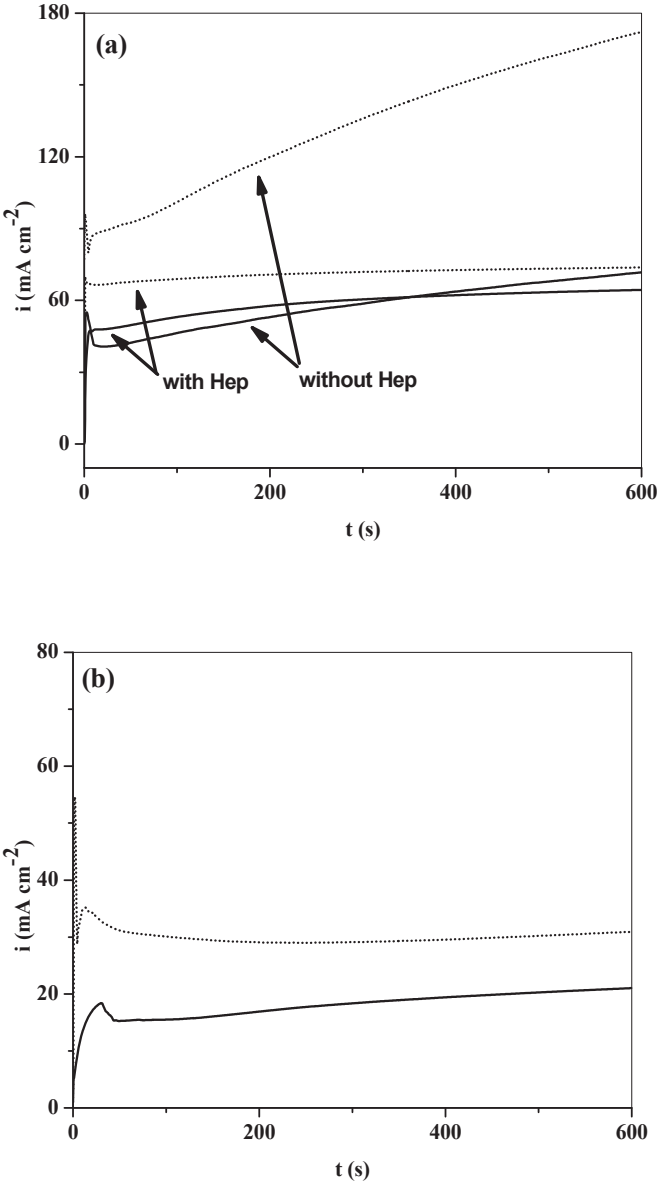

Fig. 4. i versus t transients obtained for NiTi alloy in the presence of 0.50 M Py solution containing 0.5 M NaSa and different Hep concentration: (a) 0.2 and (b) 0.4 g L^{-1}. In solid line the transients obtained at 1.0 V (SCE) and in dotted line the transients obtained at 1.5 V (SCE) for all Hep concentrations.

concentration in g L^{-1} of Hep and y the molar (M) concentration of Sa. If the electrosynthesis was performed in the presence of both anions (Hep and Sa) the film will be named as $PPy_{xHep+ySa}$. In these cases, well defined i versus t transients were obtained which grow with time (Figs. 3 and 4). According to Fig. 3, a potential increase from 1.0 to 1.5 V (SCE) produces an increase in the anodic polymerization charge for all Hep concentrations. Furthermore, for the same applied potential value, an increase in the Hep concentration produces an increase in the polymerization charge. A total NiTi surface coverage with PPy was achieved only when the applied potential was 1.5 V (SCE).

The polymerization charges are much higher in the presence of both dopants as compared to the synthesis performed only for a given Hep concentration for the same applied potential value (Fig. 4 versus Fig. 3). This is an expected result. However, an increase in the Hep concentration causes a reduction of the polymerization charge at both applied potentials. The polymerization charge calculated from the area under i vs. t curves obtained for different electrolyte solutions and at different applied potentials is summarized in Table 1.

In the case of the PPy bilayer synthesized on NiTi alloy, the first layer was formed at 0.9 V(SCE) in solutions of 0.50 M Py containing 0.50 M NaSa and the second layer at 1.5 V(SCE) in solutions of 0.50 M Py containing 0.2 g L^{-1} Hep. The PPy bilayer will be named as $PPy_{0.5Sa}/PPy_{0.2Hep}$.

In all cases, the PPy films formed under potentiostatic control onto NiTi alloy can be removed only by abrasion with emery paper.

In order to characterize the morphology of the PPy films formed under potentiostatic control, SEM micrographs for the three different cases were obtained (Fig. 5). The $PPy_{0.2Hep}$ film presents the typical granular morphology with an average grain size of 150 nm (Fig. 5a), which increases to 300 nm for the higher Hep concentration. Moreover, the $PPy_{0.2Hep+0.5Sa}$ film, doped with Hep and Sa, shows a complex structure where hollow rectangular microtubes, the typical granular morphology and needle type

Table 1
Polymerization charge calculated from the area under i vs. t curves obtained in different electrolyte solutions and at different applied potentials.

Electrosynthesis solution	Applied Potential during 600 s (V vs. SCE)	Polymerization Charge (C cm^{-2})
0.2 g L^{-1} Hep + 0.5 M Py	1.0	0.332
	1.5	0.979
0.3 g L^{-1} Hep + 0.5 M Py	1.0	0.415
	1.5	1.142
0.4 g L^{-1} Hep + 0.5 M Py	1.0	0.576
	1.5	2.023
0.2 g L^{-1} Hep + 0.5 M NaSa + 0.5 M Py	1.0	35.209
	1.5	42.701
0.4 g L^{-1} Hep + 0.5 M NaSa + 0.5 M Py	1.0	10.826
	1.5	18.013
0.5 M NaSa + 0.5 M Py	1.0	34.491
	1.5	79.720

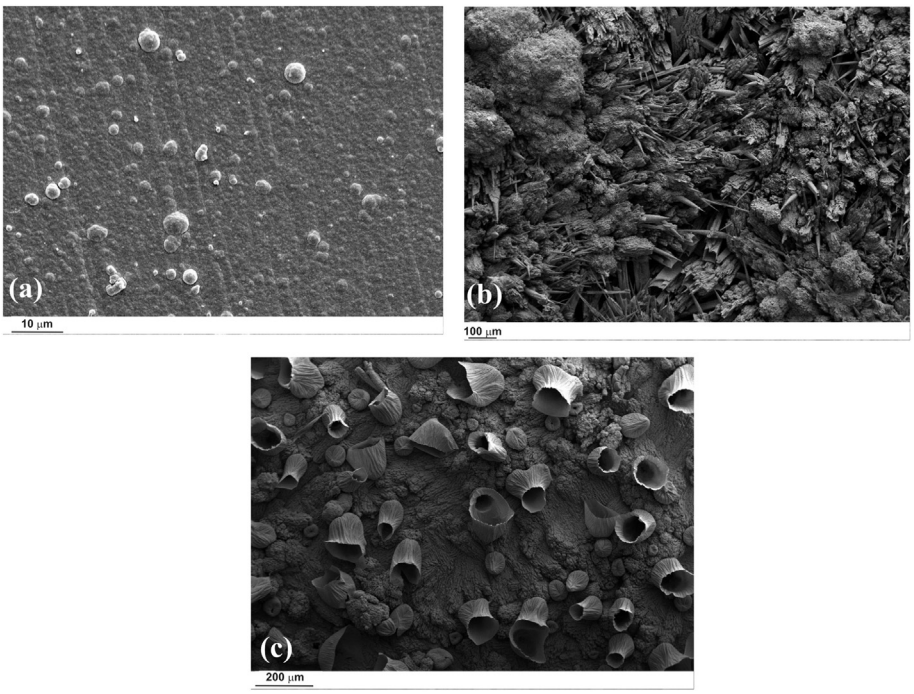

Fig. 5. SEM micrographs obtained at different magnifications for PPy films formed on NiTi alloy at different conditions: (a) PPy film obtained at 1.5 V(SCE) during 1800 s in 0.5 M Py + 0.2 g L^{-1} Hep solution ($PPy_{0.2Hep}$), (b) PPy film obtained at 1.5 V(SCE) during 1800 s in 0.5 M Py + 0.2 g L^{-1} + 0.5 M NaSa solution ($PPy_{0.2Hep+0.5Sa}$) and (c) PPy bilayer obtained at 0.9 V(SCE) during 600 s in 0.5 M Py + 0.5 M NaSa solution (first layer) and at 1.5 V(SCE) during 1800 s in 0.5 M Py + 0.2 g L^{-1} Hep solution (second layer) ($PPy_{0.5Sa}$/$PPy_{0.2Hep}$).

deposits coexist (Fig. 5b) [23]. On the other hand, the $PPy_{0.5Sa}$/$PPy_{0.2Hep}$ bilayer has a first layer of hollow rectangular microtubes of PPy doped with Sa, which is covered with a PPy layer of granular morphology doped with Hep. Cup-type microcontainers uniformly distributed over the entire surface can also be observed (Fig. 5c). This kind of morphology has been previously reported for PPy where the simultaneous formation of O_2 bubbles during electrosynthesis is responsible for this type of structure [24]. The growth of PPy doped with Hep around these O_2 bubbles template results in the microstructures described above. It is important to note that this type of PPy microstructure was not observed when the electropolymerization substrate was the bare alloy. In this case gas bubbles release from the surface of the working electrode is negligible to the naked eye. In the case of bilayer, the higher surface area of $PPy_{0.5Sa}$ film produces more active sites for oxygen evolution reaction.

In order to determine the presence of Hep in the different PPy films, EDX analysis was performed (Fig. 6). The presence of S signal in the EDX spectra of $PPy_{0.2Hep}$ film (Fig. 6a) and $PPy_{0.5Sa}$/$PPy_{0.2Hep}$ bilayer (Fig. 6b) indicate that Hep is retained in the polymer matrix to maintain the electrical neutrality. On the contrary, the EDX spectrum of $PPy_{0.2Hep+0.5Sa}$ film (Fig. 6c) does not show S signal. Considering that Sa concentration in solution is higher than that of Hep, it is possible that the polymer was only doped with Sa in order to maintain electrical neutrality, or that the concentration of Hep in the film is so low that it cannot be detected by this technique.

The decrease in the electropolymerization charge as the Hep concentration increases (Fig. 4) should be related with changes in the polymer morphology. The electropolymerization charge depends on the surface area of the growing polymer. The relative amount of hollow rectangular microtubes which have a larger surface area, decreases as the Hep concentration increases.

The different electrosynthesized PPy films were carefully scrapped of the NiTi alloy surface and analyzed by FT-IR spectroscopy. Fig. 7 shows the vibrational spectra of $PPy_{0.2Hep}$ (curve a) and $PPy_{0.2Hep+0.5Sa}$ (curve b) films dispersed in KBr discs. The

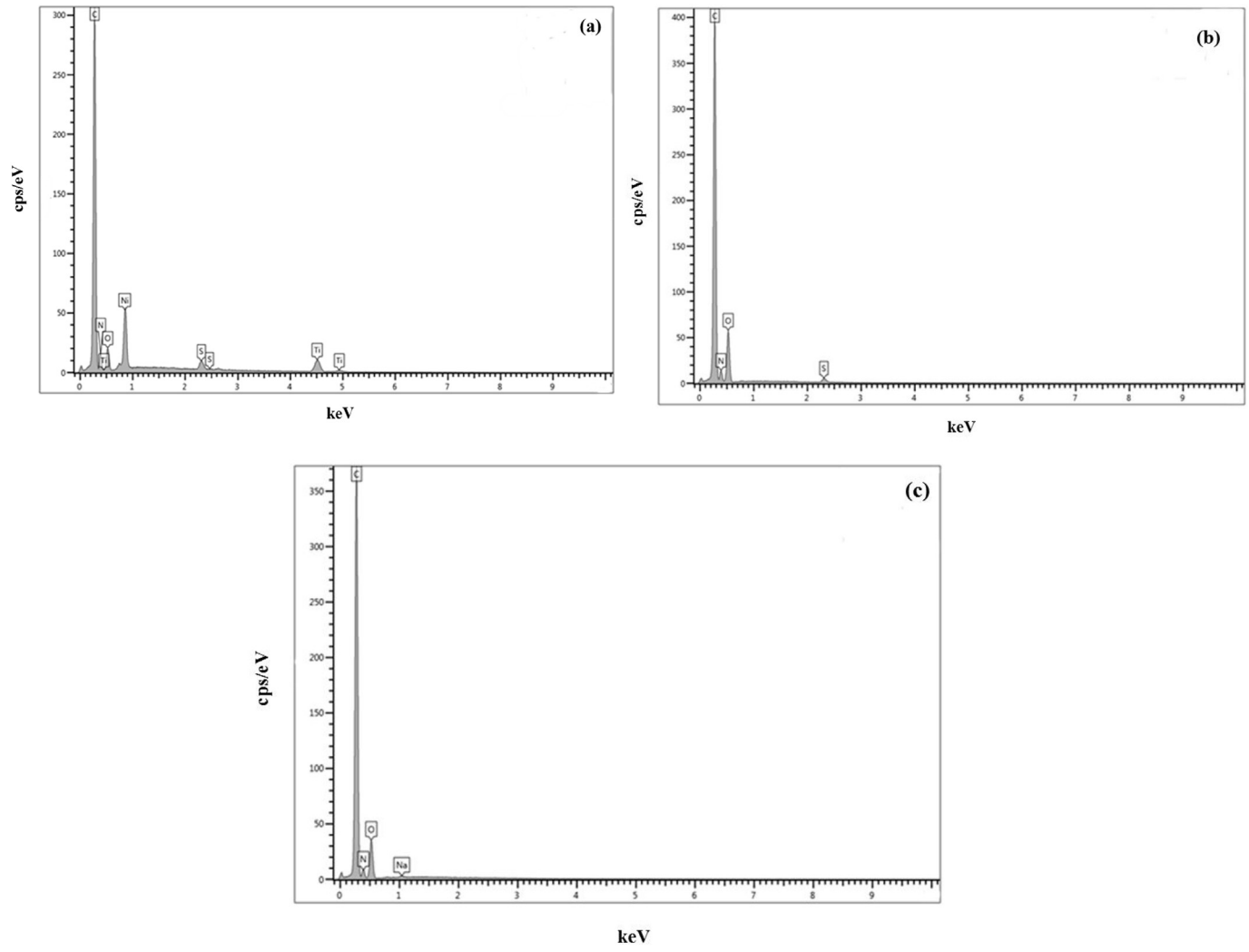

Fig. 6. EDX spectra of NiTi alloy coated with: (a) $PPy_{0.2Hep}$, (b) $PPy_{0.5Sa}/PPy_{0.2Hep}$ and $PPy_{0.2Hep+0.5Sa}$ films.

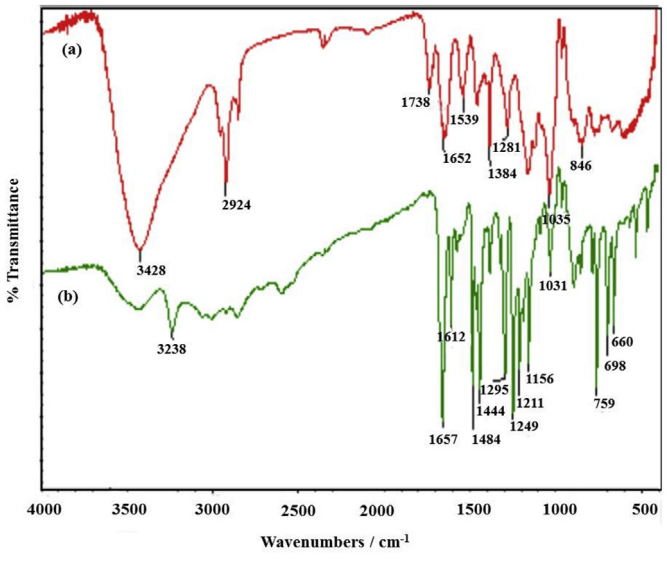

Fig. 7. FT-IR spectra (KBr) of electrodeposited PPy films detached from the NiTi alloy surface. (a) $PPy_{0.2Hep}$ and (b) $PPy_{0.2Hep+0.5Sa}$ films.

assignments of the bands have been made considering previous vibrational studies of the PPy and of the dopants. The spectrum of $PPy_{0.2Hep}$ film (Fig. 7, curve a) shows all the bands associated with the presence of the polypyrrole [25–27] and those due to heparin [28]. The absorption bands due to heparin's CH and CH_2 appear at 2924 and 1852 cm^{-1}. The 1652 cm^{-1} band is assigned to the C=C stretching motion in the PPy ring. The asymmetric stretching vibrations bands of S-O appear at 1281 and 1164 cm^{-1} while the band attributable to the stretching vibrations of the S=O bonds of N-sulfate groups could be observed at 1035 cm^{-1}. The spectrum of $PPy_{0.2Hep+0.5Sa}$ film is dominated by the vibrational bands of salicylate which masked the weaker heparin signals (Fig. 7, curve b). A weak band is observed at 3238 cm^{-1} (OH stretching vibrations) [27,29]. The salicylate bands appear at the same wavenumbers than those previously reported and discussed by our group for $PPy_{0.5Sa}$ film [27]. Both spectra can be observed in Fig. 8. On the other hand, no differences were observed between the spectra of $PPy_{0.2Hep+0.5Sa}$ films (Fig. 7, curve b) and $PPy_{0.5Sa}/PPy_{0.2Hep}$ bilayer (not shown here). It is an expected result, since both spectra show the presence of polypyrrole and salicylate.

3.2. Corrosion behavior

One of the objectives of the present study was to evaluate the

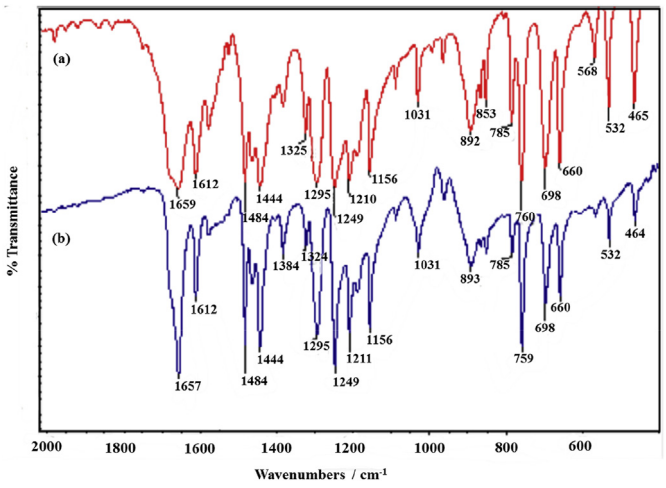

Fig. 8. FT-IR spectra (KBr) of electrodeposited PPy films. (a) $PPy_{0.5Sa}$ film electrosynthesized on 316 L stainless steel [27] and (b) $PPy_{0.2Hep+0.5Sa}$ film detached from the NiTi alloy surface.

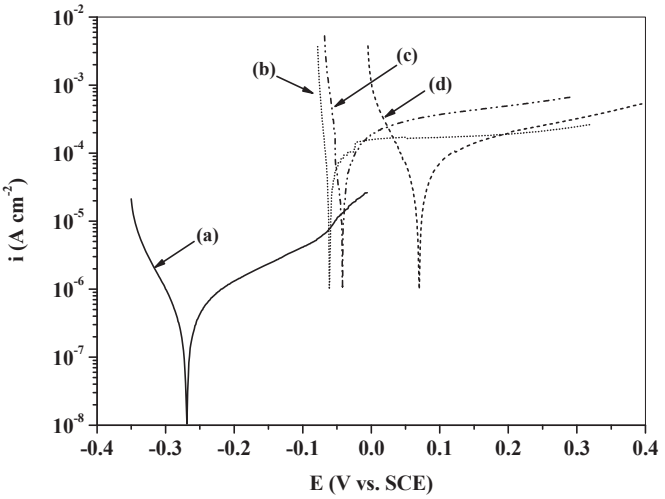

Fig. 10. Tafel curves registered in Ringer's solution after OCP measurements for: (a) uncoated and NiTi alloy coated with: (b) $PPy_{0.2Hep}$, (c) $PPy_{0.2Hep+0.5Sa}$ and (d) $PPy_{0.5Sa}$/$PPy_{0.2Hep}$ films. Sweep rate: 0.001 V s^{-1}.

corrosion resistance of the coated NiTi alloy in Ringer's solution. The variation of OCP with time can be used as an estimation of the protection grade imparted by the PPy coating. This measure was taken for $PPy_{0.2Hep}$ and $PPy_{0.2Hep+0.5Sa}$ films and $PPy_{0.5Sa}$/$PPy_{0.2Hep}$ bilayer. For a comparative purpose, the OCP variation with time of uncoated NiTi alloy was also considered (Fig. 9). As can be seen in Fig. 9, there is a shift in the OCP value towards more positive potential values when the electrode was coated by PPy. This behavior suggests an anodic protection mechanism exerted by the conductive polymer, wherein the bilayer coating has the greatest degree of corrosion protection in Ringer's solution.

Tafel plots were obtained after OCP stabilization (3600 s) starting from −0.20 V(SCE) to 0.20 V(SCE) vs. OCP with a potential scan rate of 0.001 V s^{-1}. For uncoated NiTi alloy, the i_{corr} value was estimated by extrapolation of anodic and cathodic Tafel lines to the E_{corr} (Fig. 10, curve a). The i_{corr} values of PPy coated NiTi alloy were estimated by extrapolation of the cathodic Tafel lines back to the corresponding values of E_{corr} (Fig. 10, curves b, c and d). According to Fig. 10, the PPy coating produces a positive shift in the corrosion potential, although the corrosion current densities measured are two orders of magnitude higher than those for the uncoated alloy (Table 2). This result can be interpreted considering that the galvanic interaction between the polymer and the substrate gives rise to oxidation of the substrate and reduction of the polymer.

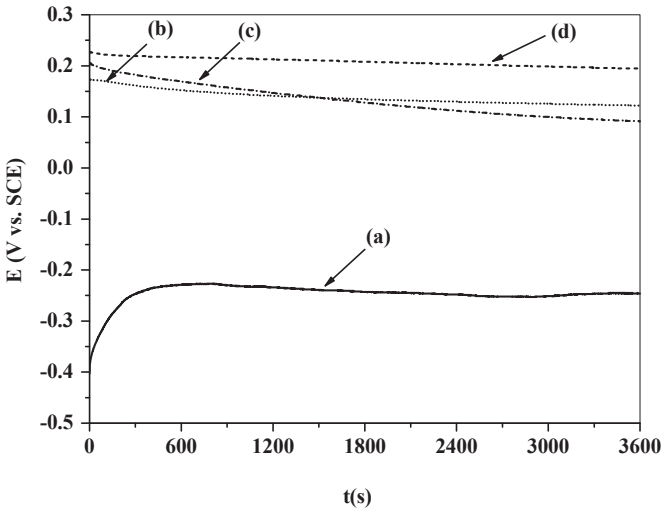

Fig. 9. Open circuit potential (OCP) vs. time plot in Ringer's solution for: (a) uncoated and NiTi alloy coated with: (b) $PPy_{0.2Hep}$, (c) $PPy_{0.2Hep+0.5Sa}$ and (d) $PPy_{0.5Sa}$/$PPy_{0.2Hep}$ films.

In order to evaluate the corrosion protection properties of the coatings, we have also recorded potentiodynamic polarization curves in Ringer's solution (Fig. 11). The uncoated NiTi alloy remains passive until 0.05 V(SCE), when the current increase indicates the onset of pitting corrosion (Fig. 11, curve a). The curves corresponding to the PPy-coated NiTi alloy present anodic peaks associated with oxidation and overoxidation of the polymers (Fig. 11, curve b, c and d). The oxygen evolution reaction takes place simultaneously with the PPy overoxidation reaction at about 1.80 V(SCE) [30]. Only the NiTi alloy coated by $PPy_{0.2Hep}$ film presents current oscillations at potentials more positive than 2.0 V(SCE), which reveals that pitting corrosion occurs (Fig. 11, curve b). Thus, the electrode covered by the other coating can be polarized at very high anodic potentials without any sign of corrosion. This can be due to the high amount of Sa available in the polymer matrix which causes a passivating effect of the underlying NiTi alloy, as was proposed in a previous paper [9].

To get an insight into the pitting corrosion protection, chronoamperometric measurements were made at 0.65 V(SCE), a potential that is higher than that necessary to initiate the localized attack of the uncoated NiTi alloy (Fig. 12). The uncoated NiTi alloy is characterized by high oscillating anodic currents which indicate localized corrosion (Fig. 12, curve a). A similar trend was observed for NiTi alloy coated by $PPy_{0.2Hep}$ film (Fig. 12, curve b), although the anodic dissolution charge involved is smaller. The NiTi alloy covered by $PPy_{0.2Hep+0.5Sa}$ films and $PPy_{0.5Sa}$/$PPy_{0.2Hep}$ bilayer act as good protective coatings considering the low currents registered (Fig. 12, curve c and d) even after 12 h of polarization. Further evidence in support of this was obtained by monitoring the released concentrations of Ni and Ti in Ringer solution after anodic polarization (Table 3). The results are consistent with a decrease of the alloy dissolution rate due to its modification with PPy film. According to these results, the pitting corrosion protection performance can be ordered in the following way: uncoated NiTi alloy < NiTi/$PPy_{0.2Hep}$ < NiTi/$PPy_{0.5Sa}$/$PPy_{0.2Hep}$ < NiTi/$PPy_{0.2Hep+0.5Sa}$.

Considering the higher resistance to pitting corrosion of NiTi

Table 2
Electrochemical parameters obtained from Tafel plots in Ringer's solution for uncoated and coated NiTi alloy.

Sample	E_{corr} (V vs. SCE)	βa (mV dec^{-1})	|βc| (mV dec^{-1})	i_{corr} (μA cm^{-2})
Bare NiTi	−0.260	307.04	111.12	0.615
NiTi/$PPy_{0.2Hep}$	−0.063	–	7.07	23.2
NiTi/$PPy_{0.5Sa}$/$PPy_{0.2Hep}$	0.067	–	18.64	10.7
NiTi/$PPy_{0.2Hep+0.5Sa}$	−0.045	–	4.38	20.8

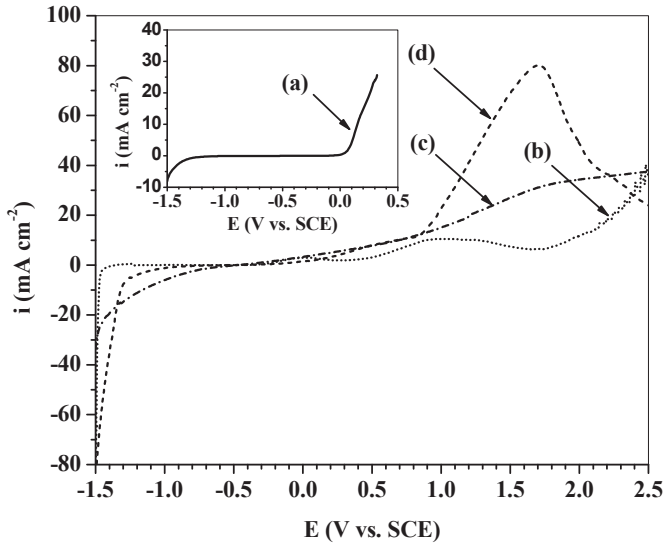

Fig. 11. LSV registered in Ringer's solution for: (a) uncoated and coated NiTi alloy with: (b) $PPy_{0.2Hep}$, (c) $PPy_{0.2Hep+0.5Sa}$ and (d) $PPy_{0.5Sa}$/$PPy_{0.2Hep}$ films. Sweep rate: 5 mV s^{-1}.

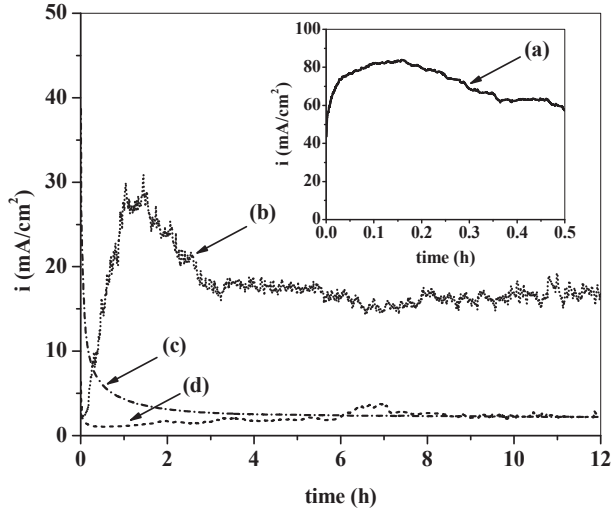

Fig. 12. Potentiostatic response obtained at 0.65 V(SCE) in Ringer solution for: (a) uncoated and coated NiTi alloy with: (b) $PPy_{0.2Hep}$, (c) $PPy_{0.2Hep+0.5Sa}$ and (d) $PPy_{0.5Sa}$/$PPy_{0.2Hep}$ films.

alloy coated with $PPy_{0.2Hep+0.5Sa}$ film, this sample and the bare alloy were analyzed by EIS at 0.65 V(SCE) in Ringer's solution at different polarization times (2 and 12 h). The Nyquist plot of uncoated NiTi alloy is shown in Fig. 13(a). A depressed semicircle with a low magnitude of impedance was obtained (Table 4). This behavior can be related with the breakdown of the passive oxide film [31], which was also observed in the Bode plot (Fig. 14(a)). The Nyquist plot of the sample coated with $PPy_{0.2Hep+0.5Sa}$ film (Fig. 13(b)) presents a depressed semicircle at high frequencies values related to the charge transfer resistance of the polymer film (kinetics control) followed in the low frequency region by a straight line with a slope of 45° attributed to a mechanism controlled by diffusion. A very similar response was obtained for a PPy film synthetized in an alkaline solution containing inorganic inhibitors ions (nitrate and molybdate) [32]. According to the Nyquist plot of the NiTi/$PPy_{0.2Hep+0.5Sa}$ sample (Fig. 13(b)), the magnitude of the impedance increases with increasing polarization time, which indicates good anticorrosion properties of the PPy coating in Ringer's solution. The same response can be observed in the Bode plot (Fig. 14(b)).

As was done previously, it is possible to estimate the double layer capacitance and charge transfer resistance from Bode plots [32]. The capacitance and charge transfer resistance values obtained for NiTi/$PPy_{0.2Hep+0.5Sa}$ sample indicate a constant capacitance and an increased charge transfer resistance with polarization time (Table 4). This can be associated with an effective corrosion protection performance of the PPy film where the passivating effect of Sa prevails, even though the structure of the polymer is porous, as was mentioned in a previous paper [9].

3.3. Anticoagulant and antiplatelet aggregating capacity

It was tested whether PPy films doped with Hep, Sa or the combination of both drugs may affect blood clotting and platelets aggregation *in vitro*. For this purpose, experimental design included exposure of each film to PPP or PRP for 35 min, and afterwards, TT, F and PA measurements were performed in fixed aliquots of each plasma.

It was found that PPy film doped with Hep prolonged TT, and that this anticoagulant effect was dependent on Hep concentration (Table 5). When F concentration was measured, no significant differences were detected respect to bare NiTi sheet (Table 5). These results are consistent with the fact that TT test evaluates the level and function of F and that thrombin is very sensitive to the presence of Hep. When PPy film doped with 0.5 M Sa were assayed, TT was prolonged and F content diminished (Table 5). The combination of both drugs elicited a synergistic effect. PPy film doped with Hep

Table 3
Concentration of Ni and Ti released after anodic polarization in Ringer's solution for uncoated and PPy-coated NiTi alloy.

Sample	Applied potential (V vs. SCE)	Time (h)	Ni concentration (mg L^{-1})	Ti concentration (mg L^{-1})
Blanck	–	–	0.015	<0.002
Bare NiTi	0.65	12	487.2	40.8
NiTi/$PPy_{0.2Hep}$	0.65	12	50.2	<0.05
NiTi/$PPy_{0.2Hep+0.5Sa}$	0.65	12	0.46	<0.05
NiTi/$PPy_{0.5Sa}$/$PPy_{0.2Hep}$	0.65	12	12.3	0.83

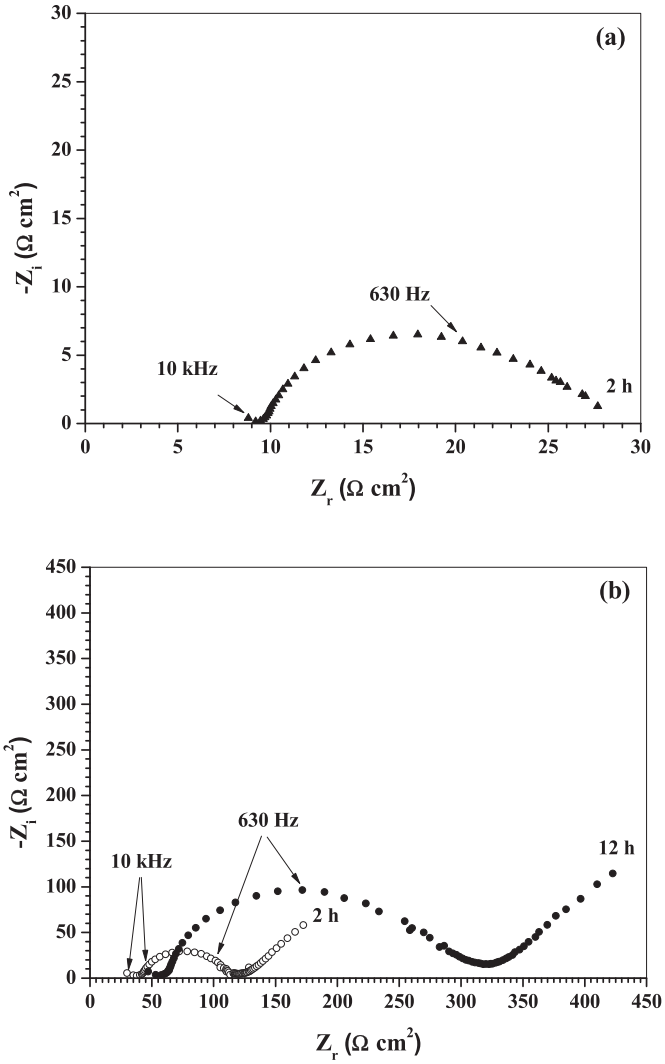

Fig. 13. Nyquist plots registered at 0.65 V(SCE) in Ringer solution for: (a) uncoated and (b) coated NiTi alloy with $PPy_{0.2Hep+0.5Sa}$ film. Polarization times are indicated.

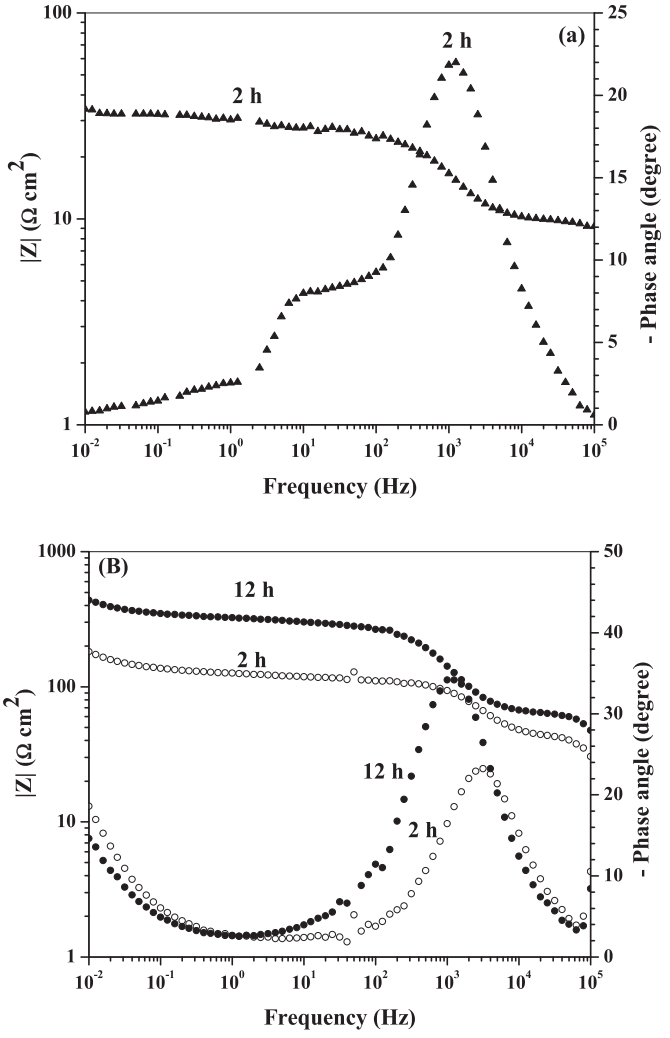

Fig. 14. Bode plots registered at 0.65 V(SCE) in Ringer solution for: (a) uncoated and (b) coated NiTi alloy with $PPy_{0.2Hep+0.5Sa}$ film. Polarization times are indicated.

and Sa exhibited a higher prolonged TT and a significant decrease in F content (Table 5).

As was expected, when PRP were incubated with PPy film doped with Sa, a significant inhibition of PA was detected (42%–90% IAP, 0.1 M – 0.5 M NaSa, respectively, $p < 0.05$). Platelet deposition on PPy film used was rule out, since platelet counting in the remaining PRP was similar to basal count (data not shown).

The identification of a useful therapeutic drugs combination for doped intravascular stents is pivotal to obtain the desire antithrombotic and antiplatelet effects. Once platelets are activated, the adherence of inflammatory cells leads to renarrowing of the blood vessel. Previous studies reported that NiTi stents coated with aluminum and polyurethane polymer possess anti-thrombogenicity properties [33]. In the present work, the dual doping Hep + Sa improved the anticoagulant properties respect to the system coated with each drug alone. The diminution in plasmatic F content and the IPA suggest a less thrombogenic condition in the microenvironment that surrounded the NiTi alloy.

The fact that the PPy film doped with both anions (Hep and Sa) improves the haemostatic features and reduces the release of nickel ions in Ringer solution suggest that NiTi/$PPy_{0.2Hep+0.5Sa}$ represents the best system considering the lower corrosion risk and the better anti-thrombogenic features.

Table 4
Double layer capacitance and charge transfer resistance values calculated for uncoated and coated NiTi alloy with $PPy_{0.5Sa+0.2Hep}$ film after polarization at 0.65 V(SCE) in Ringer's solution.

Sample	Polarization time (h)	C (μF cm^{-2})	R (Ω cm^2)
Bare NiTi	2	22.07	26.85
NiTi/$PPy_{0.2Hep+0.5Sa}$	2	1.40	71.68
NiTi/$PPy_{0.2Hep+0.5Sa}$	12	1.41	225.68

4. Conclusions

The electrodeposition of granular PPy film onto NiTi alloy was successfully carried out in a neutral Hep solution using potentiodynamic and potentiostatic techniques. The addition of Sa anion in the electrosynthesis solution produced a PPy film with a complex structure where hollow rectangular microtubes, the typical granular morphology and needle type deposits coexist. It was also possible to generate a PPy bilayer constituted by a single layer of hollow rectangular microtubes of PPy doped with Sa, which was covered with a PPy layer doped with Hep with a granular morphology and cup-type microcontainers uniformly distributed

Table 5
Haemostatic parameters measured for different doped PPy films.

Sample	Bare NiTi	$PPy_{0.2Hep}$	$PPy_{0.3Hep}$	$PPy_{0.4Hep}$	$PPy_{0.5Sa}$	$PPy_{0.5Sa+0.2Hep}$
TT (sec)	15 ± 1.1	25 ± 3.1*	30 ± 8.1*	60 ± 11.8*	35 ± 9.9*	58 ± 20.0*
F (sec)	313 ± 4.4	302 ± 65.6	334 ± 15.9	311 ± 61.4	274 ± 11.2*	163 ± 47.8*

Thrombin time (TT) and fibrinogen (F) concentration measurements were assessed after 35 min of incubation (37 °C). Results represent the means of three independent experiments (n = 2).
Values of TT and F of PPP incubated without the devices were: 14.8 ± 1.2 and 320 ± 5.1, respectively.
*$p < 0.05$.

over the entire surface. The adhesion between all PPy coatings and the NiTi alloy surface was good and they can be only removed by mechanical abrasion.

The PPy coating formed onto NiTi alloy in solution containing Hep and Sa anions presents the best pitting corrosion protection in Ringer solution and the better anti-thrombogenic properties, which would result in a promising film used as a biocompatible material.

Acknowledgments

The financial support of the Secretaría de Ciencia y Técnica - UNS (PGI 24/M146), the Consejo Nacional de Investigaciones Científicas y Técnicas (CONICET- PIP 112-201101-00055) and the Agencia Nacional de Promoción Científica y Tecnológica (ANPCYT PICT-2012-0141) is gratefully acknowledged.

References

[1] T. Duerig, A. Pelton, D. Stöckel, An overview of nitinol medical applications, Mater. Sci. Eng. A 273–275 (1999) 149–160.
[2] X. Liu, P.K. Chu, C. Ding, Surface modification of titanium, titanium alloys, and related materials for biomedical applications, Mater. Sci. Eng. R 47 (2004) 49–121.
[3] S. Shabalovskaya, J. Anderegg, J. Humbeeck, Critical overview of nitinol surfaces and their modifications for medical applications, Acta Biomater. 4 (2008) 447–467.
[4] B. O'Brien, W.M. Carroll, M.J. Kelly, Passivation of nitinol wire for vascular implants-a demonstration of the benefits, Biomaterials 23 (2002) 1739–1748.
[5] D. Starosvetsky, I. Gotman, Corrosion behavior of titanium nitride coated Ni–Ti shape memory surgical alloy, Biomaterials 22 (2001) 1853–1859.
[6] S. Zein El Abedin, U. Welz-Biermann, F. Endres, A study on the electrodeposition of tantalum on NiTi alloy in an ionic liquid and corrosion behaviour of the coated alloy, Electrochem. Comm. 7 (2005) 941–946.
[7] N.K. Guimard, N. Gomez, C.E. Schmidt, Conducting polymers in biomedical engineering, Prog. Polym. Sci. 32 (2007) 876–921.
[8] M.B. González, S.B. Saidman, Electrosynthesis of hollow polypyrrole microtubes with a rectangular cross-section, Electrochem. Commun. 13 (2011) 513–516.
[9] M. Saugo, D.O. Flamini, L.I. Brugnoni, S.B. Saidman, Silver deposition on polypyrrole films electrosynthesised onto nitinol alloy, corrosion protection and antibacterial activity, Mat. Sci. Eng. C 56 (2015) 95–103.
[10] I.L. Meek, M.A.F.J. van de Laar, H.E. Vonkeman, Non-steroidal anti-inflammatory drugs: an overview of cardiovascular risks, Pharmaceuticals 3 (2010) 2146–2162.
[11] E.M. Muñoz, R.J. Linhardt, Heparin-binding domains in vascular biology, Arterioscler. Thromb. Vasc. Biol. 24 (2004) 1549–1557.
[12] E. Seyrek, P. Dubin, Glycosaminoglycans as polyelectrolytes, Adv. Colloid Interface Sci. 158 (2010) 119–129.
[13] J. Hirsh, S.S. Anand, J.L. Halperin, V. Fuster, Mechanism of action and pharmacology of unfractionated heparin, Arterioscler. Thromb. Vasc. Biol. 21 (2001) 1094–1096.
[14] G. Wood, J. Iroh, Effect of electrolytes and process parameters on the electropolymerization of pyrrole onto carbon fibers, J. Appl. Polym. Sci. 61 (1996) 519–528.
[15] R.M. Cornelius, J. Sanchez, P. Olsson, J.L. Brash, Interactions of antithrombin and proteins in the plasma contact activation system with immobilized functional heparin, J. Biomed. Mater. Res. A 67 (2003) 475–483.
[16] D. Zhou, C.O. Too, G.G. Wallace, Synthesis and characterisation of polypyrrole/heparin composites, React. Funct. Polym. 39 (1999) 19–26.
[17] X. Yang, C.O. Too, L. Sparrow, J. Ramshaw, G.G. Wallace, Polypyrrle-heparin system for the separation of thrombin, React. Funct. Polym. 53 (2002) 53–62.
[18] K.-H. Park, E.A. Jo, K. Na, Heparin/polypyrrole (PPy) composite on gold-coated matrix for the neurite outgrowth of PC12 cells by electrical stimulation, Biotechnol. Bioprocess Eng. 12 (2007) 463–469.
[19] J.S. Moreno, S. Panero, B. Scrosati, Electrochemical polymerization of polypyrrole-heparin nanotubes: kinetics and morphological properties, Electrochem. Acta 53 (2008) 2154–2160.
[20] R. Ma, K.N. Sask, C. Shi, J.L. Brash, I. Zhitomirsky, Electrodeposition of polypyrrole-heparin and polypyrrole-hydroxyapatite films, Mater. Lett. 65 (2011) 681–684.
[21] E.M. Stewart, X. Liu, G.M. Clark, R.M.I. Kapsa, G.G. Wallace, Inhibition of smooth muscle cell adhesion and proliferation on heparin-doped polypyrrole, Acta Biomater. 8 (2012) 194–200.
[22] N. Ferraz, D.O. Carlsson, J. Hong, R. Larsson, B. Fellström, L. Nyholm, M. Stromme, A. Milhranyan, Haemocompatibility and ion exchange capability of nanocellulose polypyrrole membranes intended for blood purification, J. R. Soc. Interface 9 (2012) 1943–1955.
[23] T. Marimuthu, S. Mohamad, Y. Alias, Needle-like polypyrrole–NiO composite for non-enzymatic detection of glucose, Synth. Met. 207 (2015) 35–41.
[24] L. Qu, G. Shi, F. Chen, Z. Jiaxin, Electrochemical growth of polypyrrole microcontainers, Macromolecules 36 (2003) 1063–1067.
[25] M.E. Nicho, H. Hu, Fourier transform infrared spectroscopy studies of polypyrrole composite coatings, Sol. Energy Mater. Sol. Cells 63 (2000) 423–435.
[26] B. Tian, G. Zerbi, Lattice dynamics and vibrational spectra of polypyrrole, J. Chem. Phys. 92 (1990) 3886–3891.
[27] M.B. González, O.V. Quinzani, M.E. Vela, A.A. Rubert, G. Benítez, S.B. Saidman, Study of the electrosynthesis of hollow rectangular microtubes of polypyrrole, Synth. Met. 162 (2012) 1133–1139.
[28] N.I. Sushko, S.P. Firsov, R.G. Zhbankov, V.M. Tsarenkov, M. Marchewka, Ch. Ratajczak, Vibrational spectra of heparin, J. Appl. Spectrosc. 61 (1994) 704–707.
[29] I.L. Lehr, O.V. Quinzani, S.B. Saidman, Comparative study of polypyrrole films electrosynthesized in alkaline and acid solutions, Mater. Chem. Phys. 117 (2009) 250–256.
[30] Tüken, Polypyrrole films on stainless steel, Surf. Coat. Technol. 200 (2006) 4713–4719.
[31] R. Oltra, M. Keddam, Application of EIS to localized corrosion, Electrochim. Acta 35 (1990) 1619–1629.
[32] D.O. Flamini, M. Saugo, S.B. Saidman, Electrodeposition of polypyrrole on nitinol alloy in the presence of inhibitor ions for corrosion protection, Corros. Sci. 81 (2014) 36–44.
[33] G. Tepe, J. Schmehl, H.P. Wendel, S. Schaffner, S. Heller, M. Gianotti, C.D. Claussen, S.H. Duda, Reduced thrombogenicity of nitinol stents—in vitro evaluation of different surface modifications and coatings, Biomaterials 27 (2006) 643–650.